Journal of Hazardous Materials 176 (2010) 617–622

Contents lists available at ScienceDirect

Journal of Hazardous Materials

journal homepage: www.elsevier.com/locate/jhazmat

Hydrothermal-hydrolysis synthesis and photocatalytic properties of nano-TiO_2 with an adjustable crystalline structure

Jinghuan Zhang, Xin Xiao, Junmin Nan*

School of Chemistry and Environment, Key Lab of Electrochemical Technology on Energy Storage and Power Generation in Guangdong Universities, South China Normal University, Guangzhou 510006, China

ARTICLE INFO

Article history:
Received 15 September 2009
Received in revised form
11 November 2009
Accepted 11 November 2009
Available online 18 November 2009

Keywords:
TiO_2
Hydrothermal method
Nanorods
Mixed crystalline
Photocatalytic activity

ABSTRACT

Tri-phase (anatase, rutile, and brookite), bi-phase (anatase and rutile), and mono-phase (rutile) TiO_2 nanomaterials with different morphologies were successively synthesized using a hydrothermal-hydrolysis method and adjusting the Ti^{4+}/Ti^{3+} molar ratio in a precursor solution. The properties of the fabricated nanomaterials were characterized using X-ray diffraction (XRD), scanning electron microscopy (SEM), transmission electron microscopy (TEM), photocatalytic reaction, and other techniques. It has been shown that TiO_2 nanorods can be obtained by increasing the Ti^{4+}/Ti^{3+} molar ratio in a precursor solution from 1:0 to 0.3:0.7. TiO_2 nanoparticles are formed if the Ti^{3+} fraction in the solution is further increased. The selective synthesis of TiO_2 nanomaterials is explained by a decrease in the reaction rate and by changes in acidity with increasing Ti^{3+} content. The tri-phase nanorods and bi-phase nanoparticles synthesized with Ti^{4+}/Ti^{3+} molar ratios from 1:0 to 0.8:0.2 and 0.2:0.8 to 0:1, respectively, have a higher degradation ability with respect to methylene blue aqueous solutions under UV irradiation at ambient temperature compared to purely rutile TiO_2 nanorods synthesized with Ti^{4+}/Ti^{3+} molar ratios from 0.7:0.3 to 0.3:0.7. The high photocatalytic activity of the multi-phase TiO_2 samples is primarily attributed to their larger band gap and suppressed recombination of photo-generated electron–hole pairs.

1. Introduction

In recent years, the semiconductor heterogeneous photocatalysis technique has attracted significant attention for solving the increasingly serious problems of environmental pollution. Compared to other semiconductor photocatalysts, titania (TiO_2) has been proven to be the most preferable material for photocatalytic processes due to its biological and chemical inertness, high photoreactivity, non-toxicity, and photostability [1–2]. The microstructure and morphology are key factors for the photocatalytic activity of TiO_2-based materials. It is generally assumed that, among the three crystalline polymorphs of TiO_2, i.e., rutile, anatase, and brookite, the anatase phase or the mixed anatase/rutile phase exhibits better photocatalytic properties. Most notably, it has been demonstrated that nano-range TiO_2 materials exhibit unique properties resulting from either an extremely large surface area-to-volume ratio or quantum confinement effects of charge carriers [3].

As a typical nanomaterial, TiO_2 nanorods synthesized by hydrothermal-hydrolysis have generated increasing interest as photocatalysts since they satisfy the requirements of having a large percentage of reactive facets and a relatively shorter conduction path. Huang and Gao [4] reported the synthesis of monodispersed rutile nanorods of 4–6 nm in diameter and up to 50–150 nm in length by hydrolysis of a $TiCl_4$ solution in concentrated HNO_3 under ambient conditions in air without the requirement for a complex apparatus. Cassaignon et al. [5] reported selective synthesis of brookite, anatase, and rutile nanoparticles by the thermohydrolysis of $TiCl_4$ in concentrated aqueous nitric acid, wherein the selectivity was strongly dependent on the medium acidity. Similarly, using aqueous solutions of $TiCl_4$ and acidic additives, Yin et al. [6] and Franklyn et al. [7] confirmed the selective formation of nanoparticulate anatase and rutile nanorods under different acidic surroundings in a hydrothermal autoclave. Moreover, the synthesis of rutile nanorods has also been reported from $TiCl_4$ in an aqueous solution with 3-hydroxytyramine as a functionalization agent [8], in hydrochloric acid–alcohol aqueous solutions [9], and in an ethanolic solution [10]. In addition, Jiu et al. [11] reported the synthesis of a pure, highly crystalline anatase phase through hydrolyzing titanium isopropoxide rather than a $TiCl_4$ precursor in the presence of an ethylenediamine basic catalyst and cetyltrimethylammonium bromide (CTAB) surfactant. Li et al. [12] synthesized TiO_2 nanorods by adding $Ti(OBu)_4$ (Bu refers to $-C_4H_9$) into the mixed solution of linoleic acid, triethylamine, and cyclohexane and then sealing the solution in a Teflon-lined stainless steel autoclave at 150 °C for 2 days. Nian and Teng [13] observed

* Corresponding author. Tel.: +86 20 39310255; fax: +86 20 39310187.
E-mail address: jmnan@scnu.edu.cn (J. Nan).

0304-3894/$ – see front matter © 2009 Elsevier B.V. All rights reserved.
doi:10.1016/j.jhazmat.2009.11.074

that a hydrothermal treatment of titanate nanotube suspensions in an acidic environment results in the formation of single-crystalline anatase nanorods with a specific crystal-elongation direction.

All of the aforementioned investigations demonstrate that precursors and solution surroundings result in a typical morphology, crystallinity, and phase composition of TiO_2 nanorods. We have synthesized multi-crystalline TiO_2 nanorods in hydrothermal autoclaving by using mixed $TiCl_4$ and $TiCl_3$ solutions without any additives as precursors. In this paper, the synthesis of TiO_2 nanorods, their physicochemical characteristics, and photocatalytic activities are presented.

2. Materials and methods

2.1. Synthesis of TiO_2 photocatalysts

All chemicals were of analytical grade and used as received without further purification. In a typical synthesis process, $TiCl_4$ and $TiCl_3$ were added in turn drop-wise into deionized water (45 mL) with magnetic stirring in an ice water bath. The total amount of Ti was 0.05 mol with various molar ratios of Ti^{4+}/Ti^{3+} (1:0, 0.9:0.1, 0.7:0.3, 0.5:0.5, 0.3:0.7, 0.1:0.9, and 0:1 and labeled as TiO_2-A, TiO_2-B, TiO_2-C, TiO_2-D, TiO_2-E, TiO_2-F, and TiO_2-G, respectively). Upon completion of the $TiCl_4/TiCl_3$ addition, the mixture was stirred in an ice bath for another 3 h, and then the resultant solution was transferred into a 50 mL Teflon-lined stainless steel autoclave until 75% of its volume was filled. The autoclave was kept in an oven at 150 °C for 48 h. After the autoclave was cooled down to room temperature, the white precipitate was first collected by filtration and then washed and dried at 100 °C.

2.2. Characterization of TiO_2 photocatalysts

The phase compositions of the as-synthesized TiO_2 samples were identified by X-ray diffraction (XRD, D/max 2200, Rigaku, Japan) with Cu Kα radiation, at 30 kV and 30 mA, and with λ = 0.154 nm. The morphology, structure, and mean diameter of samples were characterized by scanning electron microscopy (SEM, JEOL JEM-5900LV, Japan) and by transmission electron microscopy (TEM, JEM-2010HR, JEOL, Japan). The average crystalline size in the samples was determined by the Scherrer equation. The specific surface area of samples was measured by nitrogen adsorption–desorption isotherms at 77 K according to the Brunauer–Emmett–Teller analysis (BET, ASAP 2020, Micromeritics, USA). A desorption isotherm was used to determine the pore size distribution using the Barrett–Joyner–Halenda (BJH) method. UV–vis diffuse reflection spectra were obtained using a UV–vis spectrophotometer (UV-2501, Shimadzu, Japan).

The photocatalytic activities of TiO_2 samples were evaluated by the degradation of methylene blue. Photocatalytic degradation was carried out in a photochemical reactor (XPA-1, Xu-Jiang Electromechanical Plant, China) equipped with a medium mercury lamp (300 W) at room temperature. All photocatalytic reactions were performed using identical initial conditions: 200 mL 5×10^{-5} mol L^{-1} methylene blue solution was mixed with 0.1 g of photocatalysts under constant magnetic stirring. Every five minutes during the reaction process, 5 mL of the methylene blue solution was taken to test the concentration of methylene blue using UV–Vis spectroscopy (λ = 668 nm).

3. Results and discussion

3.1. Structure and morphology of TiO_2 photocatalysts

The XRD patterns of the TiO_2 photocatalysts synthesized under different molar ratios of Ti^{4+}/Ti^{3+} in the precursor solution are shown in Fig. 1. With increasing Ti^{3+} content, it was observed that anatase and brookite diffraction peaks steadily became weaker and then disappeared completely when the molar ratio of Ti^{4+}/Ti^{3+} was changed from 0.7:0.3 to 0.3:0.7. The anatase diffraction peaks appeared again and became stronger, whereas the intensities of the rutile diffraction peaks became weaker when the molar ratio of Ti^{4+}/Ti^{3+} varied from 0.2:0.8 to 0:1. Therefore, it can be concluded that TiO_2 samples synthesized in different Ti^{4+}/Ti^{3+} solutions present different crystalline phases. Samples TiO_2-A and TiO_2-B contained all three crystalline phases: anatase (PDF card 71-1169, JCPDS), rutile (PDF card 87-0120, JCPDS) and brookite (PDF card 29-1360, JCPDS). Samples TiO_2-C, TiO_2-D, and TiO_2-E contained a pure rutile phase. Samples TiO_2-F and TiO_2-G contained anatase and rutile phases. Hence, tri-phase (anatase, rutile, and brookite), bi-phase (anatase and rutile), and mono-phase (pure rutile) TiO_2 samples can be obtained by simply adjusting the molar ratio of the Ti^{4+}/Ti^{3+} in precursor solutions.

In previous works [5–7], it was pointed out that the selective synthesis of brookite, anatase, and rutile nanoparticles by the thermohydrolysis of $TiCl_4$ was strongly dependent on the acidity of the medium. The results presented in Fig. 1 validate the possibility of synthesizing multi-phase TiO_2 materials and also indicate that the hydrolyzing surroundings can be adjusted by changing the molar ratio of Ti^{4+}/Ti^{3+}. It was found that the initial pH values of precursor solutions increase with increasing $TiCl_3$ content in the solution, which might affect the formation of TiO_2 crystals and, correspondingly, lead to the appearance or disappearance of peaks of anatase, rutile, and brookite. The phase contents of anatase, rutile, and brookite in the TiO_2 composites are shown in Table 1 and have been calculated from the integrated intensities of the anatase (1 0 1), rutile (1 1 0), and brookite (1 2 1) peaks with the following formulas [14,15]:

$$W_A = \frac{K_A A_A}{K_A A_A + A_R + K_B A_B}, \quad (1)$$

$$W_R = \frac{A_R}{K_A A_A + A_R + K_B A_B)}, \quad (2)$$

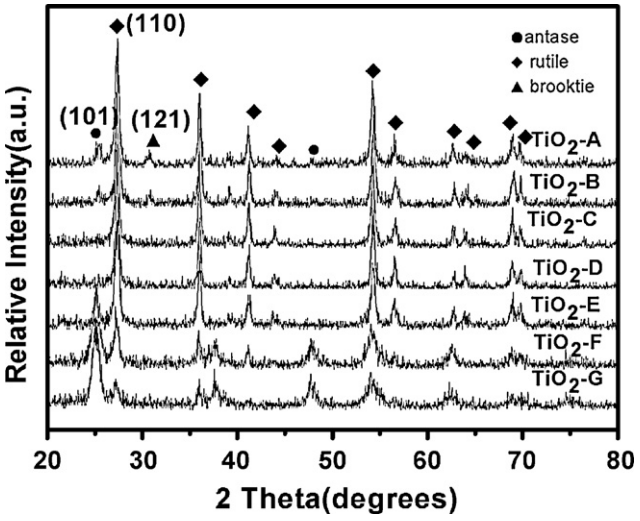

Fig. 1. XRD patterns of TiO_2 samples synthesized under different Ti^{4+}/Ti^{3+} precursor solutions. The molar ratios of Ti^{4+}/Ti^{3+} for samples TiO_2-A to TiO_2-G are 1:0, 0.9:0.1, 0.7:0.3, 0.5:0.5, 0.3:0.7, and 0.1:0.9, respectively.

Table 1
Summary of the physicochemical properties of TiO_2 samples synthesized with different Ti^{4+}/Ti^{3+} molar ratios in the precursor solutions.

Abbr. of samples	Molar ratio of Ti^{4+}/Ti^{3+}	Crystalline size (nm)[a]	Anatase content (%)[b]	Rutile content (%)[b]	Brookite content (%)[b]	S_{BET} ($m^2\,g^{-1}$)[c]	Pore size (nm)[d]	Pore volume ($mL\,g^{-1}$)[e]
TiO_2-A	1:0	20.3	11.4	67.6	21.0	45	11.86	0.1333
TiO_2-B	0.9:0.1	26.7	8.4	71.3	20.3	41	15.57	0.1633
TiO_2-C	0.7:0.3	21.1	–	100	–	42	16.04	0.1701
TiO_2-D	0.5:0.5	18.3	–	100	–	47	17.55	0.2076
TiO_2-E	0.3:0.7	16.6	–	100	–	63	17.51	0.2328
TiO_2-F	0.1:0.9	9.8	54.5	44.5	–	127	9.56	0.2559
TiO_2-G	0:1	8.5	72.3	27.7	–	133	10.4	0.2944

[a] Calculated using the Scherrer formula.
[b] Calculated using formulas in Refs. [14,15].
[c] BET surface area calculated from the linear part of the BET plot.
[d] BJH desorption average pore diameter (4 V/A).
[e] Single point total pore volume of the pores at $P/P_0 = 0.97$.

$$W_B = \frac{K_B A_B}{K_A A_A + A_R + K_B A_B}, \quad (3)$$

where W_A, W_R, and W_B represent the weight fractions of the anatase, rutile, and brookite phases, respectively. A_A, A_R, and A_B are the integrated intensities of the anatase (1 0 1), rutile (1 1 0), and brookite (1 2 1) peaks, respectively. The variables K_A and K_B are coefficients with values 0.886 and 2.721, respectively [14,15].

According to the phase contents of the TiO_2 samples shown in Table 1 and their synthesis conditions, it can be concluded that the formation of the multi-crystalline TiO_2 occurs due to the following two factors. The first is that gradual growth is necessary for the formation of a single-phase system. The reaction rate of TiO_2 formation with Ti^{4+} ions is too fast to attain thermodynamic equilibrium under the condition of a high molar ratio of Ti^{4+}. Thus, more nuclei may be formed in a solution system, which subsequently results in the formation of multi-phase resultants due to a high degree of supersaturation. In contrast, heterogeneous nucleation occurs when the degree of supersaturation is controlled by a low level of Ti^{4+} [16,17]. A slow reaction rate can be maintained with an increasing molar ratio of Ti^{3+} because Ti^{3+} must be first oxidized to Ti^{4+} in order to form a TiO_2 crystal. This slow oxidation by dissolved oxygen results in the preferential formation of large single crystals (pure rutile) with a thermodynamic equilibrium shape. The second

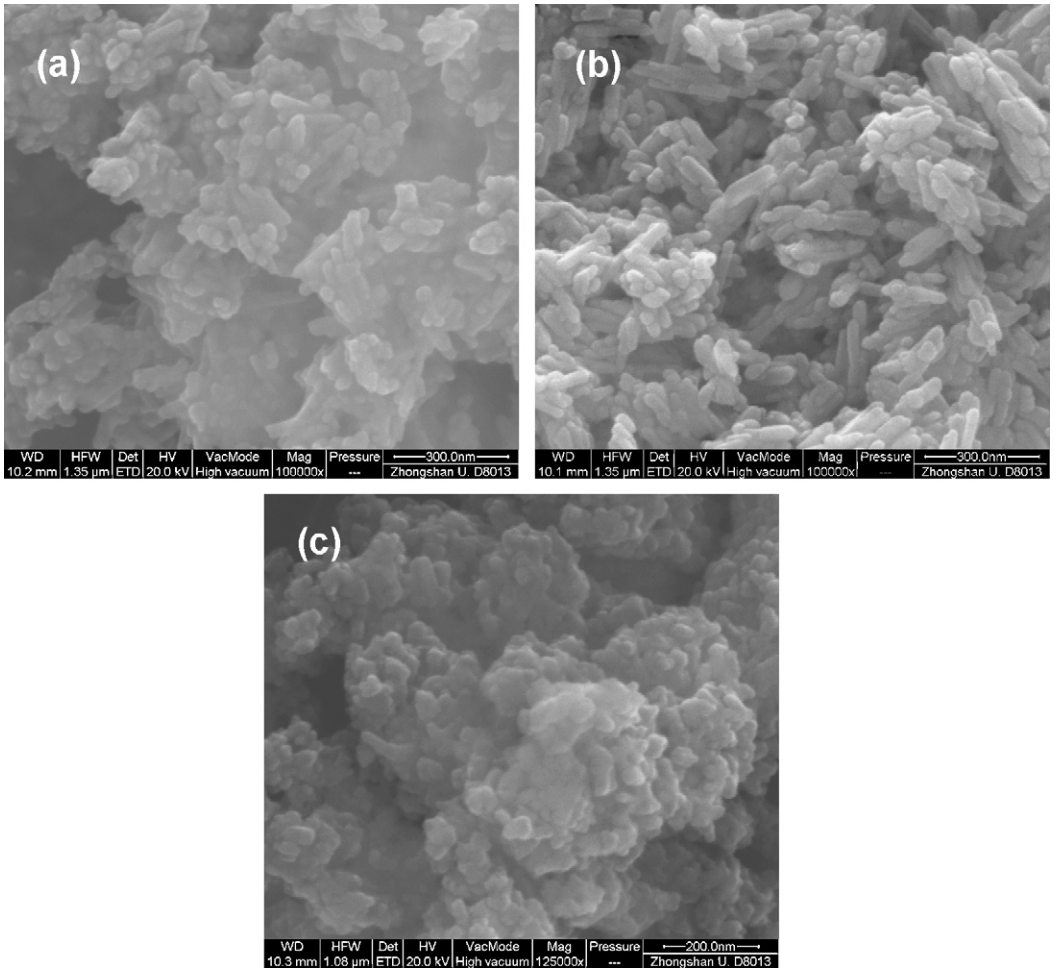

Fig. 2. SEM images of (a) TiO_2-A, (b) TiO_2-B, and (c) TiO_2-F.

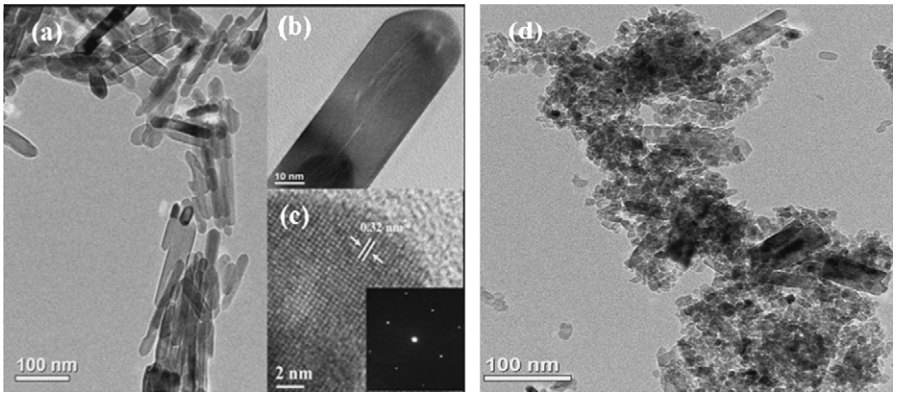

Fig. 3. TEM micrographs of TiO_2-B and TiO_2-F samples: (a) overview image of TiO_2-B, (b) and (c) HRTEM images of TiO_2-B. The inset in (c) shows an electron diffraction pattern of a TiO_2 nanorod. (d) Overview image of TiO_2-F.

factor is related to the pH of the precursor solutions [18]. Generally speaking, anatase is easily formed in a solution with a relatively high pH, while rutile requires a low pH [19]. A large amount of $TiCl_3$ can provide a relatively high pH, which is one of the key reasons why samples TiO_2-F and TiO_2-G retain anatase as their main phase.

The crystalline sizes of TiO_2 composites calculated by the Scherrer equation [20] ($\Phi = K\lambda/\beta\cos\theta$, where Φ is the crystallite size, $\lambda = 0.154$ nm is the wavelength of the X-ray irradiation, K is usually taken to be equal to 0.89, β is the peak width at half-maximum height, and θ is the diffraction angle of the (1 0 1) peak) are also shown in Table 1. In general, the crystalline sizes of TiO_2 composites decrease with increasing Ti^{3+} contents in the precursor solutions, although the crystalline sizes of samples TiO_2-B and TiO_2-C are slightly larger than that of TiO_2-A, which are attributed to their difference of crystal structure formed under different precursor solutions.

SEM and TEM studies reveal that an increasing $TiCl_3$ content in precursor solutions influences the morphology of TiO_2 samples. By varying the Ti^{4+}/Ti^{3+} molar ratio from 1:0 to 0.3:0.7, TiO_2 nanorods could be obtained, while mixtures of nanorods and nanoparticles were produced when the molar ratio of Ti^{4+}/Ti^{3+} was varied from 0.3:0.7 to 0:1. Especially in comparison with the sample synthesized in a Ti^{4+} solution (Fig. 2a), more regular TiO_2 nanorods were obtained after the addition of a certain amount of Ti^{3+}. Three typical SEM images of TiO_2 samples synthesized under different Ti^{4+}/Ti^{3+} molar ratios are shown in Fig. 2. The SEM images of TiO_2 samples synthesized under molar ratios from 0.9:0.1 to 0.3:0.7 are similar to the image in Fig. 2b, while Fig. 2c is representative of molar ratios from 0.2:0.8 to 0:1. The images also show that the morphologies of TiO_2 samples correspond to their phase compositions and preparation conditions.

The TiO_2 nanorods and nanoparticles shown in Fig. 2 appear to be stuck together; however, separated nanorods and nanoparticles can be observed in TEM images that show that the contact force between the TiO_2 nanorods or nanoparticles is weak, although no dispersant was added into the precursor solution during the reaction process. Fig. 3 shows TEM images of TiO_2 nanorods and nanoparticles obtained from samples TiO_2-B and TiO_2-F and presents typical morphologies of TiO_2 samples synthesized under these precursor conditions.

An overview of sample TiO_2-B at a low magnification (Fig. 3a) shows that it almost exclusively contains nanorods with lengths of 80–200 nm and diameters of 25–35 nm. The corresponding high-resolution TEM (HRTEM) images are displayed in Fig. 3b and c. The mono-crystalline nature of the nanorods with a perfect rutile structure is clearly visible. The fringe spacing parallel to the main axis of the nanorod is estimated to be 0.32 nm, similar to the findings of Huang and Gao [4] and Tahir et al. [8]. This is close to the (1 1 0) lattice spacing of the rutile phase, indicating that crystal growth is preferentially in the (1 1 0) direction, which results in the anisotropic growth of the nanocrystals, leading to elongated nanoparticles (nanorods) [8]. Furthermore, the diffraction pattern shown in the inset of Fig. 3c (taken from a corresponding nanorod) is consistent with the rutile phase. An overview of sample TiO_2-F at a low magnification in Fig. 3d shows that it contains a small quantity of nanorods and a mass of nanoparticles, which indicates that the formation of nanorods could be prevented if precursor solutions containing an excess of Ti^{3+} ions were used.

The nitrogen adsorption-desorption isotherm and Barret–Joyner–Halenda (BJH) pore size distribution analyses were carried out to characterize the surface states of the TiO_2 samples, with typical results shown in Fig. 4. The curves corresponding to samples TiO_2-A and TiO_2-D display type II adsorption-desorption isotherms, which are typical characteristics of macroporous materials. These macropores can be formed through the interaggregation of nanorods. The curves corresponding to samples TiO_2-F and TiO_2-G are type IV isotherms (BDDT classification) [18,21]. At high relative pressures from 0.6 to 1.0, the isotherms exhibit type H3 hysteresis loops that can be associated with aggregates of plate-like particles that give rise to narrow slit-like pores [18,21], which indicates that the samples contain mesoporous (2–50 nm) structures. The formation of mesoporous structures for samples TiO_2-F and TiO_2-G is attributed to the aggregation of TiO_2 nanoparticles. As the molar fraction of the Ti^{3+} ions was

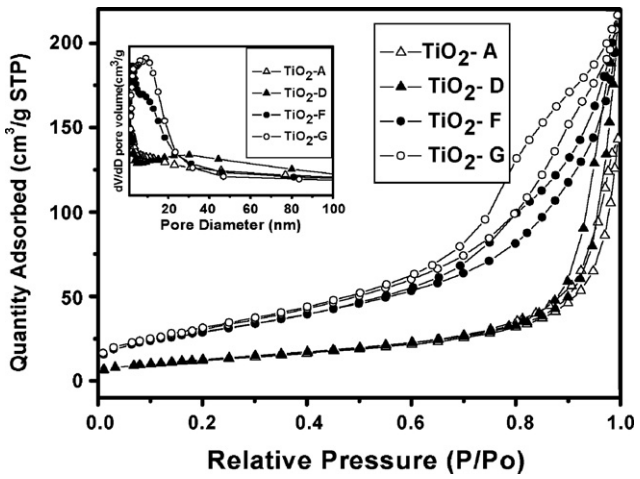

Fig. 4. Nitrogen adsorption–desorption isotherms and Barret–Joyner–Halenda (BJH) pore size distribution plots (inset) of the TiO_2-A, TiO_2-D, TiO_2-F, and TiO_2-G samples.

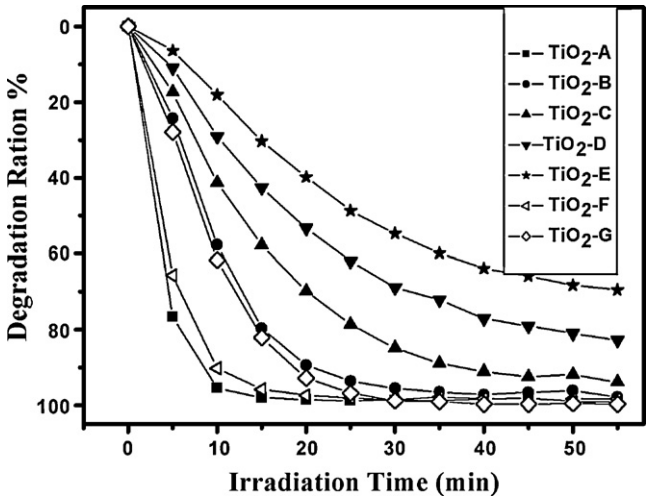

Fig. 5. Photocatalytic degradation ratios of methylene blue vs. irradiation time using TiO_2 samples synthesized in different Ti^{4+}/Ti^{3+} precursor solutions. Molar ratios of Ti^{4+}/Ti^{3+} for TiO_2-A to TiO_2-G are 1:0, 0.9:0.1, 0.7:0.3, 0.5:0.5, 0.3:0.7, and 0.1:0.9, respectively.

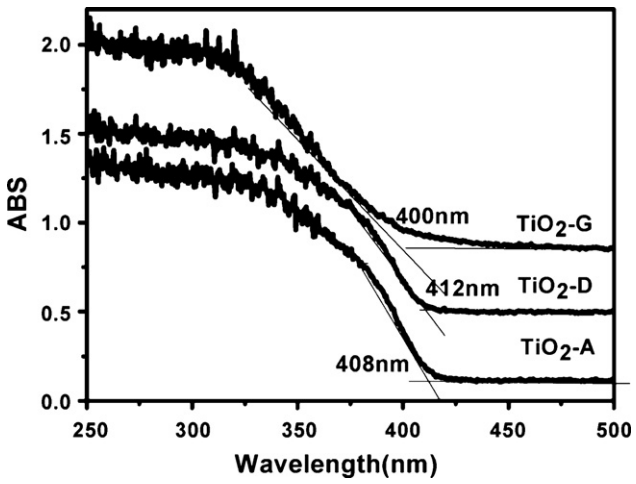

Fig. 6. UV–vis diffuse reflectance spectra of samples TiO_2-A, TiO_2-D and TiO_2-G.

increased, the hysteresis loops shifted towards smaller relative pressures, and the areas of the hysteresis loops gradually became bigger. The BET surface area, pore parameter, and pore volume of the as-prepared samples are summarized in Table 1. Concerning the data presented in Table 1, it is considered that the BET surface areas of the TiO_2 nanorods are curved in their morphologies, and the smaller BET surface area of the TiO_2 nanorods compared to that of the nanoparticles can be ascribed to a more regular morphology of the nanorods.

3.2. Photocatalytic activities of the TiO_2 photocatalysts

Fig. 5 shows the degradation ratio of methylene blue vs. irradiation time using the as-synthesized TiO_2 photocatalysts. Samples synthesized with different Ti^{4+}/Ti^{3+} precursor solutions present different photocatalytic activities corresponding to their physicochemical properties. Samples TiO_2-A, TiO_2-B, TiO_2-F, and TiO_2-G show much higher photocatalytic activities compared to samples TiO_2-C, TiO_2-D, and TiO_2-E.

It is generally accepted that the activities of TiO_2 photocatalysts depend on a large number of parameters, including phase structure, specific surface area and crystalline size [2,20–23]. Combined with the results presented in Fig. 1 and Table 1, the different photocatalytic activities of these TiO_2 photocatalysts can be attributed to their phase structures and specific surface areas. Previous reports indicate that composite photocatalytic materials with mixed crystalline structures have higher reactivities because their specific crystalline structures lead to a suppressed recombination of electron–hole pairs [22,23]. The band gaps of the brookite, rutile, and anatase phases are 3.4, 3.0, and 3.2 eV [15], respectively. As indicated above, samples TiO_2-A and TiO_2-B are tri-phase (anatase, rutile, and brookite) and thus present higher photocatalytic activities due to their larger useful band gaps, and correspondingly, they exhibit more powerful redox abilities [23], although they have lower specific surface areas.

Similarly, samples TiO_2-F and TiO_2-G are composed of two phases (anatase and rutile), which can suppress the recombination of electron–hole pairs and, consequently, enhance photocatalytic activity [24]. Therefore, the narrow band gap of the rutile phase will absorb photons with longer wavelengths, while electrons and holes excited in the rutile phase will not easily recombine due to their transfer into the anatase phase. In addition, the large specific surface areas of samples TiO_2-F and TiO_2-G explain why they demonstrated high photocatalytic activities. Samples TiO_2-C, TiO_2-D, and TiO_2-E exhibited low photocatalytic activities because they contain only the rutile phase, regular nanorod morphologies, and relatively smaller specific surface areas.

The UV–vis diffuse reflectance spectra of the TiO_2 samples were recorded to obtain insight into their light absorption characteristics, and typical results are shown in Fig. 6. In comparison to samples TiO_2-A and TiO_2-D, sample TiO_2-G shows a stronger absorption in the 250–325 nm range and a blue shift in the band gap transition, which can be attributed to differences in crystallite size and the phase structure of the samples. The increased absorption at wavelengths less than 390 nm is known to be caused by electron excitations from the valence band to the conduction band of TiO_2 [15]. The adsorption edge shift towards shorter wavelengths in the sequence of TiO_2-D, TiO_2-A, and TiO_2-G clearly indicates a gradual increase of the band gap. The band gap energies are calculated according to the following formula [25]:

$$Eg\ (\mathrm{eV}) = \frac{1240}{\lambda g}, \tag{4}$$

where λg is the wavelength corresponding to the intersection point of the vertical and horizontal parts of the spectra in Fig. 6. Thus, samples TiO_2-A, TiO_2-D, and TiO_2-G Exhibit 3.04, 3.0, and 3.1 eV band gap energies, respectively. The band gap of brookite is 3.4 eV [15], which is higher than that of anatase or rutile, and can explain the fact that the band gaps of samples TiO_2-A and TiO_2-G are slightly larger than that of TiO_2-D. The larger band gap of sample TiO_2-G compared to that of TiO_2-A can be ascribed to a significantly smaller brookite phase content of sample TiO_2-A. These data agree well with those reported by Luo et al. [26] and also with the above photocatalytic results. It can be concluded that the general differences in the photocatalytic activities of these TiO_2 samples are obvious, although it is not easy to compare their photocatalytic activities by using the full spectrum of the Hg lamp (from 250 nm to the visible region), taking into account that these catalysts absorb light in different wavelength regions.

4. Conclusions

Tri-phase (anatase, rutile, and brookite), bi-phase (anatase and rutile), and pure rutile TiO_2 nanomaterials with nanorod and nanoparticle morphologies have been successfully synthesized in a hydrothermal autoclave through simple adjustments of the Ti^{4+}/Ti^{3+} molar ratios in the precursor solutions. Nanorods and nanoparticles can be synthesized by increasing the Ti^{4+}/Ti^{3+} molar

ratios from 1:0 to 0.3:0.7 and 0.2:0.8 to 0:1, respectively. It is considered that the formation of nanorods takes place due to the slower reaction rate associated with increasing molar fractions of Ti^{3+} because Ti^{3+} must first be oxidized to Ti^{4+} in order to form a TiO_2 crystal. A change in the acidity of the precursor solutions is another key factor. Tri-phase TiO_2 nanorods and bi-phase TiO_2 nanoparticles exhibit higher degradation abilities to methylene blue aqueous solutions compared to purely rutile TiO_2 nanorods under irradiation from a medium mercury lamp at ambient temperatures, which can be mainly attributed to their mixed crystalline structure, larger useful band gap, and suppressed recombination of electron–hole pairs.

Acknowledgements

This study was financially supported by the Natural Science Funds of Department of Education (Grand No. 05Z008) and the Science and Technology Projects (Grand No. 2007B030101007) of Guangdong Province.

References

[1] R. Asahi, T. Morikawa, T. Ohwaki, K. Aoki, Y. Taga, Visible light photocatalysis in nitrogen-doped titanium oxides, Science 293 (2001) 269–271.
[2] X.B. Chen, S.S. Mao, Titanium dioxide nanomaterials: synthesis, properties, modifications, and applications, Chem. Rev. 107 (2007) 2891–2959.
[3] X.B. Chen, S.S. Mao, Synthesis of titanium dioxide (TiO_2) nanomaterials, J. Nanosci. Nanotechnol. 6 (2006) 906–925.
[4] Q. Huang, L. Gao, A simple route for the synthesis of rutile TiO_2 nanorods, Chem. Lett. 32 (2003) 638–639.
[5] S. Cassaignon, M. Koelsch, J.P. Jolivet, Selective synthesis of brookite, anatase and rutile nanoparticles: thermolysis of $TiCl_4$ in aqueous nitric acid, J. Mater. Sci. 42 (2007) 6689–6695.
[6] H.B. Yin, Y. Wada, T. Kitamura, T. Sumida, Y. Hasegawa, S. Yanagida, Novel synthesis of phase-pure nano-particulate anatase and rutile TiO_2 using $TiCl_4$ aqueous solutions, J. Mater. Chem. 12 (2002) 378–383.
[7] P.J. Franklyn, D.C. Levendis, C. Demetrius, N.J. Coville, M. Maaza, Phase transformation of hydrothermally synthesized nanoparticle TiO_2: from anatase to rutile nanorods, S. Afr. J. Chem. 60 (2007) 71–75.
[8] M.N. Tahir, P. Theato, P. Oberle, G. Melnyk, S. Faiss, U. Kolb, A. Janshoff, M. Stepputat, W. Tremel, Facile synthesis and characterization of functionalized, monocrystalline rutile TiO_2 nanorods, Langmuir 22 (2006) 5209–5212.
[9] W. Wang, B.H. Gu, L.Y. Liang, W.A. Hamilton, D.J. Wesolowski, Synthesis of rutile (α-TiO_2) nanocrystals with controlled size and shape by low-temperature hydrolysis: effects of solvent composition, J. Phys. Chem. B 108 (2004) 14789–14792.
[10] Y.W. Wang, L.Z. Zhang, K.J. Deng, X.Y. Chen, Z.G. Zou, Low temperature synthesis and photocatalytic activity of rutile TiO_2 nanorod superstructures, J. Phys. Chem. C 111 (2007) 2709–2714.
[11] J.T. Jiu, S. Isoda, F.M. Wang, M. Adachi, Dye-sensitized solar cells based on a single-crystalline TiO_2 nanorod film, J. Phys. Chem. B 110 (2006) 2087–2092.
[12] X.L. Li, Q. Peng, J.X. Yi, X. Wang, Y.D. Li, Near monodisperse TiO_2 nanoparticles and nanorods, Chem. Eur. J. 12 (2006) 2383–2391.
[13] J.N. Nian, H. Teng, Hydrothermal synthesis of single-crystalline anatase TiO_2 nanorods with nanotubes as the precursor, J. Phys. Chem. B 110 (2006) 4193–4198.
[14] H.Z. Zhang, J.F. Banfield, Understanding polymorphic phase transformation behavior during growth of nanocrystalline aggregates: insights from TiO_2, J. Phys. Chem. B 104 (2000) 3481–3487.
[15] J.C. Yu, L.Z. Zhang, J.G. Yu, Direct sonochemical preparation and characterization of highly active mesoporous TiO_2 with a bicrystalline framework, Chem. Mater. 14 (2002) 4647–4653.
[16] B.C. Bunker, P.C. Rieke, B.J. Tarasevich, A.A. Campbell, G.E. Fryxell, G.L. Graff, L. Song, J. Liu, W. Virden, G.L. Mcvay, Ceramic thin film formation of functionalized interfaces through biomimetic processing, Science 264 (1994) 48–55.
[17] E. Hosono, S. Fujihara, H. Imai, I. Honma, I. Masaki, H. Zhou, One-step synthesis of nano-micro chestnut TiO_2 with rutile nanopins on the microanatase octahedron, ACS Nano 1 (2007) 273–278.
[18] J.G. Yu, Y.R. Su, B. Cheng, M.H. Zhou, J. Mole, Effects of pH on the microstructures and photocatalytic activity of mesoporous nanocrystalline titania powders prepared via hydrothermal method, Catal. A: Chem. 258 (2006) 104–112.
[19] S. Yamabi, H. Imai, Crystal phase control for titanium dioxide films by direct deposition in aqueous solutions, Chem. Mater. 14 (2002) 609–614.
[20] D.S. Kim, S.Y. Kwak, The hydrothermal synthesis of mesoporous TiO_2 with high crystallinity thermal stability, large surface area, and enhanced photocatalytic activity, Appl. Catal. A: Gen. 323 (2007) 110–118.
[21] K.S.W. Sing, D.H. Everett, R.A.W. Haul, L. Moscou, R.A. Pierotti, J. Rouquerol, T. Siemieniewska, Reporting physisorption data for gas/solid systems with special reference to the determination of surface area and porosity, Pure Appl. Chem. 57 (1985) 603–619.
[22] R.R. Bacsa, J. Kiwi, Effect of rutile phase on the photocatalytic properties of nanocrystalline titania during the degradation of p-coumaric acid, Appl. Catal. B: Environ. 16 (1998) 19–29.
[23] T. Ohno, K. Tokieda, S. Higashida, M. Matsumura, Synergism between rutile and anatase TiO_2 particles in photocatalytic oxidation of naphthalene, Appl. Catal. A: Gen. 244 (2003) 383–391.
[24] M. Koelsch, S. Cassaignon, J.F. Guillemoles, J.P. Joliver, Comparison of optical and electrochemical properties of anatase and brookite TiO_2 synthesized by the sol–gel method, Thin Solid Films 403–404 (2002) 312–319.
[25] B. Oregan, M. Gratzel, A low-cost, high-efficiency solar cell based on dye-sensitized colloidal TiO_2 films, Nature 353 (1991) 737–739.
[26] H.M. Luo, C. Wang, Y.S. Yan, Synthesis of mesostructured titania with controlled crystalline framework, Chem. Mater. 15 (2003) 3841–3846.